# Experimental Measurements of the Effective Thermal Conductivity and Contact Resistance of Compressed and Uncompressed Metal Foam for Applications to Cold Plates

Bolape Alade<sup>1</sup>, \*Alfonso Ortega<sup>1</sup>, Metodi Zlatinov<sup>2</sup>, Denver Schaffarzick<sup>2</sup>

<sup>1</sup>NSF – Center for Energy-Smart Electronic Systems, Villanova University, Villanova, PA, USA

<sup>2</sup>ERG Aerospace Corporation, Oakland, CA, USA

\*alfonso.ortega@villanova.edu

Abstract—Open-cell metal foams have attractive properties such as high surface area density and moderate pressure drop such that they are under exploration as an alternative to traditional finned structures in air-cooled heat sinks or liquid-cooled cold plates for electronics cooling. Recent studies in metal foam technology have shown that mechanical compression decreases the foam porosity and increases the surface area density, both of which increase the thermal performance of a metal foam cold plate under the right conditions. The current study focuses on experimental measurements of the effective thermal conductivity of compressed metal foam, motivated by applications using single and two-phase liquid flow. Experimental measurements are reported for the effective thermal conductivity and contact resistance of compressed and uncompressed copper, aluminum, and silicon carbide foams. An ASTM standard two-bar method was used with the two-sample technique in which two samples of different thicknesses are measured under identical conditions to extract both the effective thermal conductivity and contact resistance. Samples of copper, aluminum and silicon carbide foams with compression ratios (CR) of 1, 2, 3, 4, and 6 were tested. It was found that previously derived experimental correlations for keff for uncompressed foam fail to capture the behavior of compressed foam. A simple correction to an existing correlation was found to successfully correlate the measured effective thermal conductivity to the solid phase thermal conductivity and sample porosity. The effective thermal conductivity for all samples increased by a factor of ten with compression leading a decrease in porosity from 90% to 50%. Similarly, thermal contact resistance without an interface material was found to also correlate with sample porosity as the number of contact areas at the solid interface increases with decreasing porosity (i.e. with increasing compression). Contact resistance was significantly decreased when a thermal interface material was used to attach the foam sample. Without the TIM, the contact resistance was a strong function of contact pressure.

#### **NOMENCLATURE**

$T_f$	Fluid temperature, <i>K</i>
$T_s$	Solid matrix temperature, <i>K</i>
$h_{sf}$	Interstitial heat transfer coefficient, $W/m^2 \cdot K$
$k_d$	Conductivity due to dispersion, $W/m \cdot K$
$k_{fe}$	Fluid effective thermal conductivity, $W/m \cdot K$
$k_{se}$	Solid effective thermal conductivity, $W/m \cdot K$
$k_{e\!f\!f}$	Foam effective thermal conductivity, $W/m \cdot K$
$k_{cu}$	Copper Thermal conductivity, $W/m \cdot K$

$A_{sf}$	Specific surface area, <i>m</i> <sup>2</sup>
$A_{contact}$	Contact area between foam and solid surface, $m^2$
$A_{apparent}$	Apparent area between foam and solid surface, $m^2$
$P_{contact}$	Contact pressure between foam and solid, psi
Q	Conduction heat flow, W
dT/dy	Temperature gradient along test column
R	Total thermal resistance, <i>K/W</i>
$R_{contact}$	Contact resistance–top and bottom interfaces, <i>K/W</i>
$R_{foam}$	Thermal resistance of the metal foam, $K/W$
$\dot{H_I}$	Thickness of the first sample, <i>m</i>
$H_2$	Thickness of the second sample, <i>m</i>
$A_c$	Foam sample or flux meter cross-sectional area, $m^2$
PPI	Pores per Inch

#### **Greek symbols**

CR

Density of metal foam material Porosity of metal foam

Compression ratio

#### I. INTRODUCTION

In various engineering applications, there is a growing emphasis on enhancing heat transfer efficiency, driven by the increasing costs of energy and materials. Employing more efficient devices not only results in reduced equipment size but also contributes to lowered maintenance expenses. In recent years, there has been an exploration of enhancing heat transfer by incorporating porous materials into thermal exchange systems. Metal foams, owing to their lightweight nature and distinctive transport properties, stand out as excellent choices for serving as thermal sinks and efficient heat exchangers. Kisitu et al. [1] studied the utilization of metal foam in twophase flow cold plates for high heat flux cooling using R134a refrigerants. Their results showed that compressed metal foam at porosities of about 50% demonstrated excellent flow boiling behavior, comparable and even exceeding conventional straight fins. The continuing study will continue this exploration in single phase (water) flow. In order to understand and model the underlying physics in both single and two-phase flows, it is necessary to understand the fundamental heat transfer mechanisms. As such, this paper will report on recent measurements of the effective thermal conductivity of copper and aluminum foams with and without compression, leading to decreases in porosity from about 90% to 50% and dramatic increase in the thermal conductivity.

In general, since being introduced to the industry, metal foams have found utility in diverse applications. These include energy transfer [2]-[4], solar collectors [5], fuel cells [6], acoustic absorption [7], [8], air-oil separation devices in jet engines [9], [10], supporting catalysts in reactors [11], hydrogen storage tanks [12] and heat exchangers [13]-[15]. Due to their expansive surface area relative to volume, the solid ligaments' high conductivity, and the flow mixing due to their intricate flow paths, metal foams excel in improving heat transfer in convective flows. As mentioned in [16], it is expected that augmentation of heat conduction within the ligaments, especially in the direction normal to the wall where heat is applied, will improve the overall heat transfer. In addition, due to the tortuous flow paths in the ligament geometry, the convective flow, whether in single or two-phases, will experience increased mixing compared to simpler channel geometries which will also increase thermal transport. In heat exchange devices, the interfacial resistance between the foam and a solid surface may be significant, depending on the thermal interface material used. Given the high porosity and irregularities on the free surface, the effective contact area at the interface with a solid surface can be low, causing a significant resistance to effective heat flow from the solid to the foam. In prior studies, the contact resistance was either combined with effective thermal conductivity ( $k_{eff}$ ), with only the latter being documented as observed in [17]-[24], or ignored altogether. Due to the disparate nature of contact resistance and thermal conductivity, it is crucial to draw a clear distinction between the two. Sadeghi et al. [25] examined the thermal interfacial resistance of aluminum foams and found a notable impact of compressive load on contact resistance and greater sensitivity to porosity as opposed to pore density.

The most common modeling approach used in prior studies to predict the convective heat transfer in metallic foams is the two-equation, non-equilibrium porous media approach. As demonstrated for example by Phanikumar and Mahajan [17], volume averaged energy equations are derived for the fluid phase, Eq. 1, and the solid phase Eq. 2.

$$(\rho c)_f \nabla T_f = \nabla \cdot \left[ \left( k_{fe} + k_d \right) \cdot \nabla T_f \right] + h_{sf} A_{sf} (T_s - T_f) \quad (1)$$

$$0 = \nabla \left[ k_{se} \cdot \nabla T_s \right] - h_{sf} A_{sf} \left( T_s - T_f \right) \tag{2}$$

Per the local non-equilibrium assumption, locally the fluid and solid temperatures are distinct. At the fluid solid interface, continuity in the heat flux is enforced through the convective heat transfer term. As seen in Eqs. 1 and 2, the fluid thermal conductivity,  $k_{fe}$ , the effective solid conductivity,  $k_{se}$ , and the

interfacial heat transfer coefficient,  $h_{sf}$ , between the foam surfaces and the fluid are the key parameters in the model. The dispersion coefficient,  $k_d$ , is introduced in order to account for the mixing in the pores that augments the molecular fluid conductivity. Several approaches have been proposed for predicting the  $k_{eff}$  of open-cell metal foams, taking into account the morphological configurations in both two and three dimensions. Calmidi and Mahajan [26] and Bhattacharya et al. [22] developed two 2D structure-based models to predict effective thermal conductivity. In these models, the arrangement of metal foam was envisioned as 2D hexagonal arrays, featuring cylindrical ligaments connected by square nodes in one model [26] and circular nodes in the other [22]. Experimental data are necessary for validating the effective thermal conductivity models. The majority of experimental data currently available are for aluminum foams. Calmidi and Mahajan [26] and Phanikumar and Mahajan [17] ascertained the effective thermal conductivities of aluminum foams saturated with both water and air, employing a steady-state methodology. These foams exhibited porosities ranging from 90% to 98%. According to their findings, the effective thermal conductivity increased dramatically as porosity decreased, although pore density did not consistently affect effective thermal conductivity.

Singh and Kasana [27] presented a simple, resistor-based model to examine the thermal pathways through their foams, drawing from existing experimental data and numerical simulations. Their model elucidated the influential role of porosity and the relative thermal conductivity of constituents in shaping the effective thermal conductivity. Using an unstable photo-thermal technique, Fetoui et al. [28] evaluated the  $k_{eff}$  of very porous aluminum foams filled with air, and their findings were consistent with those of Calmidi and Mahajan [26]. Sadeghi et al. [25] investigated aluminum foams, assessing the influence of different porosities and pore densities under diverse compression conditions. The findings revealed that, although foam porosity had an impact on effective thermal conductivity, it exhibited minimal sensitivity to compression forces lower than 2 MPa. Dyga and Witczak [29] conducted experiments on the effective thermal conductivities of aluminum foams when filled with oil, water, and air. Their findings revealed a marked difference in the influence of heat transfer through the filling fluid on  $k_{eff}$ , particularly when comparing foams saturated with liquid to those saturated with air. It is important to highlight that the efforts mentioned above are solely focused on aluminum foams, with minimal experimental exploration conducted on foams made from other metals. Xiao et al. [30], [31] carried out experimental research on the  $k_{eff}$  of copper and nickel foams. However, their study focused on solid paraffin as the filling material for the foams. In summary, the available literature data for effective thermal conductivity is predominately for high porosity aluminum foam. Evidently, more data are needed for copper foam, and for foams with lower porosities as produced by mechanical compression, given their significant applications in numerous fields [21], [32], [33].

#### II. OBJECTIVES

To the author's knowledge, the current study is the first to examine the effects of foam compression on the effective thermal conductivity of metal foams. The objective of the current research is to measure the effective thermal conductivity ( $k_{eff}$ ) and thermal interfacial resistance ( $R_{contact}$ ) at various compression ratio (CR) of 1, 2, 3, 4, and 6 for copper, aluminum, and silicon carbide foams. Compression ratio is the ratio of volume of uncompressed foam to volume of compressed. A second research objective is to determine if existing correlations for effective thermal conductivity are adequate for foams at lower porosities produced by foam compression.

#### III. EXPERIMENTAL MEASUREMENTS

### A. Test Foam Samples

Figure 1(a) displays a scanning electron microscope (SEM) image depicting the structure of copper foam. The realistic metal foam is composed of multiple representative cells, comprising ligaments and nodes. In Figure 1(b) and Figure 1(c), SEM images reveal the structures of uncompressed and compressed copper foam with CR of 2 and 4 used in this research. It is clearly seen that compression collapses the foam structure, causing a denser, lower porosity medium.

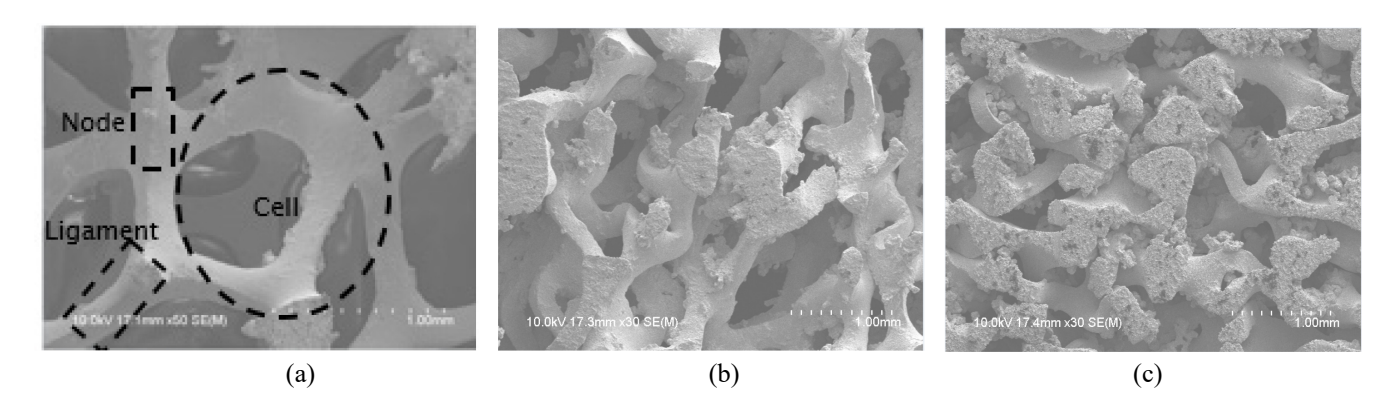


Fig. 1. SEM image of open-cell copper foam: (a) uncompressed copper foam with porosity of 90%; (b) copper foam with CR = 2 and porosity of 80%; (c) copper foam with CR = 4 and porosity of 60%.



Fig. 2: Test metal foams of different thickness but same microstructure

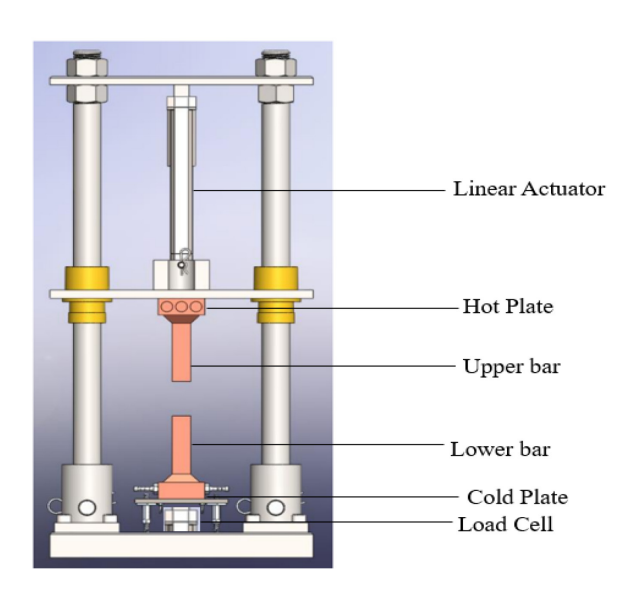


Fig. 3. Schematic of test section

Fig. 2 shows copper foam samples of two thicknesses utilized in the thermal conductivity measurements. investigation utilized ERG Duocel copper, aluminum, and silicon carbide foams characterized by distinct porosities but consistent pore density. The Duocel foams were made using an ERG proprietary method; the finished foam has the exact same composition as the basic alloy. The foams were formed from copper alloys C101, aluminum alloys Al6101, and silicon carbide alloy SiC. The metal foams were compressed by ERG to various levels of compression and were not bonded to metal face sheets. The samples had a cross-section of 2.54 x 2.54 cm (1 in. x 1 in.) with various thicknesses. The sample specifications are tabulated in Table 1. In this work, copper foam samples with pore densities of 40 PPI and porosity ranges of 60-92%, aluminum foam samples with pore densities of 40 PPI and porosity ranges of 50-94%, silicon carbide foam sample with pore densities of 60 PPI and porosity ranges of 85% were used. The porosity and pore densities were measured by ERG using standard diagnostics.

# B. ASTM Thermal Conductivity Tester

The samples were tested in the ASTM thermal conductivity tester shown in Fig. 3. The test samples are loaded between the heated bar and the cold bar shown in the figure. The copper bars have cross-sectional area of 2.54 x 2.54 cm (1 in. x 1 in.). The upper bar is attached to a support plate that can move smoothly in the vertical direction on two brass bushings sliding on the polished guide bars. The support plate is attached to a linear actuator which provides programmable motion and loading in the vertical direction. Heat is generated in the hot plate by three cylindrical Calrod heaters. The cold plate is made of serpentine channels machined into an aluminum block. Cooling is provided by a constant temperature circulating water bath featuring a programmable coolant temperature. Standard 100% oxygen-free copper material was used to fabricate the bars. This is important because the thermal conductivity of the copper bars is used in the data reduction, hence, it is necessary

to use a known, NIST traceable, material for the bars. Four T-type thermocouples were affixed to each copper bar at 6 mm spacing, as shown in Fig. 4. These temperature measurements were used to determine the temperature gradient through each bar. The heat flow rate through the foam sample and the surface temperature at the interface between the copper bars and the sample were determined using the measured temperature gradient, as illustrated in Fig. 4.

# C. Data Acquisition Procedure

After preparation of the thermal interface material, the sample was placed on the top of the cold bar, and the upper heated bar was lowered until in came into contact with the sample. The loading force was monitored by the load cell under the cold plate assembly. The linear actuator was continuously actuated to keep the loading pressure level at the required level. For the studies reported here, loading pressure of 15 and 30 psi were utilized as will be reported in a subsequent section. The circulating deionized water temperature and electrical heater power from a direct current power supply were set to 10°C and 15 Watts, respectively. Data were acquired after steady state conditions were achieved. The time required varied depending on the sample attributes but typically was about four hours. After steady state was achieved, the temperatures on the hot and cold bars were acquired with an Agilent 34970a data acquisition system.

The data reported here are for foam samples in air. Sadeghi et al. [25] stated that due to the significantly low thermal conductivity of air, its impact on the effective thermal conductivity can be negligible. Previous models, by Boomsma and Poulikakos [18], required additional assumptions regarding the heat flow through the composite medium and the porous medium itself. Assuming uniformity in the porous medium, effects of heat transfer by natural convection and radiation within the pores were deemed to negligible for this study.

Table 1: Characteristics of the C	cu, Al, and SiC foam	samples under study
-----------------------------------	----------------------	---------------------

	Copper			Aluminum						SiC
CR	1	2	4	1	1	2	3	4	6	1
Porosity	0.92	0.81	0.64	0.91	0.94	0.84	0.77	0.71	0.50	0.85
Pore density (PPI)	40	40	40	40	40	40	40	40	40	60
Thickness (mm)	2.5	2.5	2.5	10	10	12.5	12.5	19	19	12.5
Thickness (mm)	10	5	5							

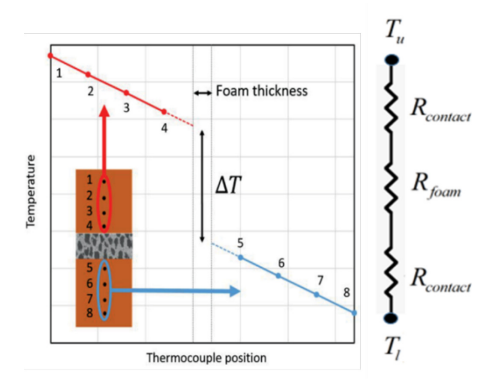


Fig. 4. Temperature distributions in two-bar apparatus with sample in between the hot and cold bar

#### D. Data Reduction

Using Fourier's law, the heat conduction through the bars may be calculated as:

$$Q = -k_{Cu}A_C \frac{dT}{dy}$$
 (3)

The temperature gradient dT/dy was determined by curvefitting the linear data and the heat flow calculated from Eq. 3. By utilizing the measured temperature gradients on both bars, it is possible to extrapolate the temperatures to the surfaces of the two bars, hence it is possible to exactly specify the thermal boundary condition on both sides of the test specimen.

The total thermal resistance includes the thermal resistance of the sample and the interfacial resistance at the upper and lower interfaces which are assumed to be equal.

$$R = \frac{\left(T_u - T_l\right)}{O} = R_{foam} + 2R_{contact} \tag{4}$$

By conducting two experiments employing materials of two different thicknesses, it is possible to extract both the effective thermal conductivity and the interfacial resistance. The results are valid if the micro-structural properties such as porosity and pore density are exactly the same for both samples, Fig. 2. At identical pressures, the contact resistances of the two samples can be considered equal due to their matching microstructure and comparable surface features on both upper and lower surfaces.

For two samples of different thickness  $H_1$  and  $H_2$ , with everything else being identical, the measured overall thermal resistances  $R_1$  and  $R_2$  are used to determine the effective conductivity as follows:

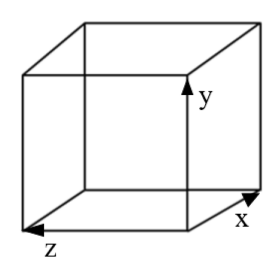


Fig. 5: Principal directions of compression relative to thermal conductivity

$$k_{eff} = \frac{\left(H_1 - H_2\right)}{(R_1 - R_2)A_C} \tag{5}$$

$$R_{contact} = \frac{\left(R_1 - \frac{H_1}{kA_C}\right)}{2} = \frac{\left(R_2 - \frac{H_2}{kA_C}\right)}{2} \tag{6}$$

Where

$$k_{eff} = \frac{H}{R_{foam} A_C} \tag{7}$$

#### E. Uncertainty Analysis

Taking into consideration Eqs. (5) and (6) for the computation of  $k_{eff}$  and  $R_{contact}$ , the essential parameters in the analysis can be expressed as:

$$k_{eff}$$
 or  $R_{contact} = f(Q, \Delta T, H, A_c)$  (8)

The primary factor introducing uncertainty in these experiments stems from errors in calculating the heat flux through the sample. The thermocouples and data collection readings exhibit maximum errors of  $\pm 0.5$  °C. To gauge uncertainty in morphology, relative densities of comparable samples with varying thicknesses were measured. The computation of the maximum uncertainty for the thermal resistance data can be carried out using the approach outlined in [34]. The highest uncertainty for this study was calculated to be  $\pm 5.2\%$ .

#### IV. RESULTS AND DISCUSSION

The thermal conductivity in the compressed foam samples is orthotropic, hence it is important to identify the thermal conductivity measured relative to the direction of compression. Using the principle directions in the sample illustrated in Fig. 5,  $k_{i,j}$  is the thermal conductivity in the i-direction, with compression in the j-direction. Hence for example,  $k_{y,y}$  refers to the thermal conductivity in the y-direction with the compression in the y-directions. The data reported in this paper should be referred to as  $k_{x,y}$ , where the compression is in the y-direction, and the thermal conductivity is in the x-direction. We note that although not experimentally proven yet, we expect that  $k_{x,y} = k_{z,y}$ , i.e. the conductivities of the compressed foam normal to the direction of compression should be the same along each principal direction. The thermal conductivity  $k_{y,y}$  will be examined in a future study.

# A. Impact of thermal interface material (TIM) on $k_{eff}$

The impact of a Thermal Interface Material (TIM) on the measured effective thermal conductivity was investigated by testing dry samples and comparing them with samples that used a thermal grease (Artic Silver) as the TIM material. The measurements for effective thermal conductivity kx,y were specifically conducted in the direction-x normal to the ydirection of compression as shown in Fig. 5. In Fig. 6, the application of 30 Psi apparent pressure with CR of 1, 2, and 4 demonstrated that the measured thermal conductivity remained consistent regardless of the TIM used. The measured contact resistance with the TIM was substantially lower than for the cases with no TIM, but the contact resistance had no demonstrable effect on the effective thermal conductivity, consistent with expectations based on the physics. The figure provides an indication of the variation in effective thermal conductivity across different porosities as compression levels vary for copper foam.

# B. Impact of Compression on $k_{eff}$

As observed in Fig. 6 for copper and Fig. 7 for aluminum, samples with CR of 4 and 6, respectively, demonstrated the highest effective thermal conductivity. This observation implies an increase in effective thermal conductivity with increased compression, or more precisely with the decreased porosity and change in ligament morphology due to compression. This observation aligns with the findings in the study by Ozmat et al. [13], which asserted that higher compressive loads, leading to larger deformations, enhance

thermal conductivity. Table 2 summarizes the effective thermal conductivity values obtained for all samples in this study.

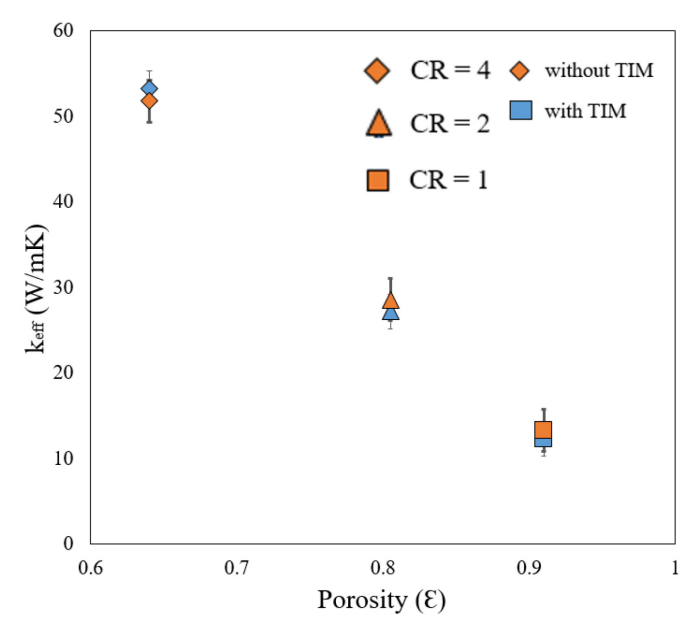


Fig. 6: Experimental data for compressed and uncompressed Cu foam effective thermal conductivity vs. porosity at 30 Psi apparent pressure

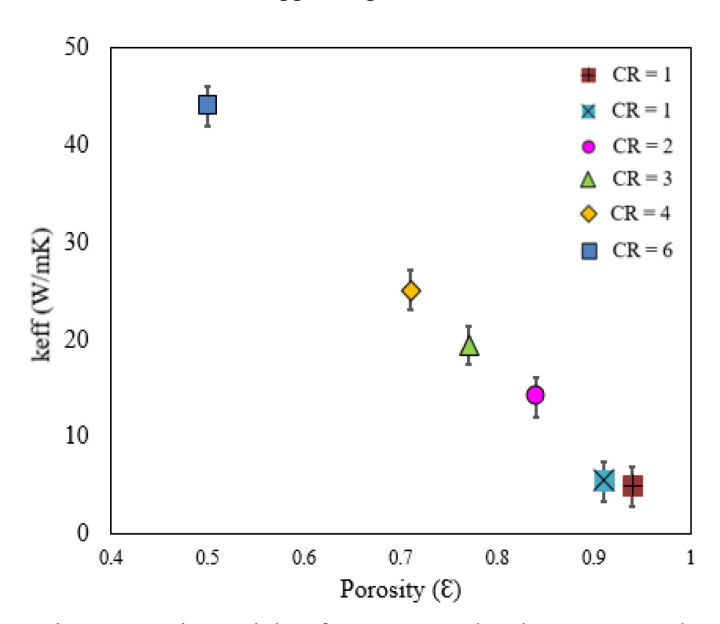


Fig. 7: Experimental data for compressed and uncompressed Al foam effective thermal conductivity vs. porosity at 30 Psi apparent pressure with TIM

Table 2. Effective thermal conductivity for uncompressed and compressed foams at 30 Psi apparent pressure

Foam Sample	Copper			Aluminum						SiC
$CR$ $k_{eff}(W/mK)$	1	2	4	1	1	2	3	4	6	1
	12.6	27.2	53.3	5.4	4.9	14.1	19.4	25.1	44.0	3.6

# C. Comparison of $k_{eff}$ to previous models

The experimental data is contrasted with established analytical models in [25], [26], [35], [36] as shown in Fig. 8 and Fig. 9 for copper foam and aluminum foam respectively. It is seen that the experimental data generally aligns with analytical models for uncompressed metal foams, i.e. foams with high porosities. However, as the compression level increases, the measured conductivity deviates from the established correlations at increasingly low porosities. Following the simple model of Sadeghi et al. [25], a new analytical model for effective thermal conductivity is proposed for compressed copper, aluminum, and silicon carbide foams:

$$k_{eff} = \frac{2}{5} (1 - \varepsilon) k_s \tag{9}$$

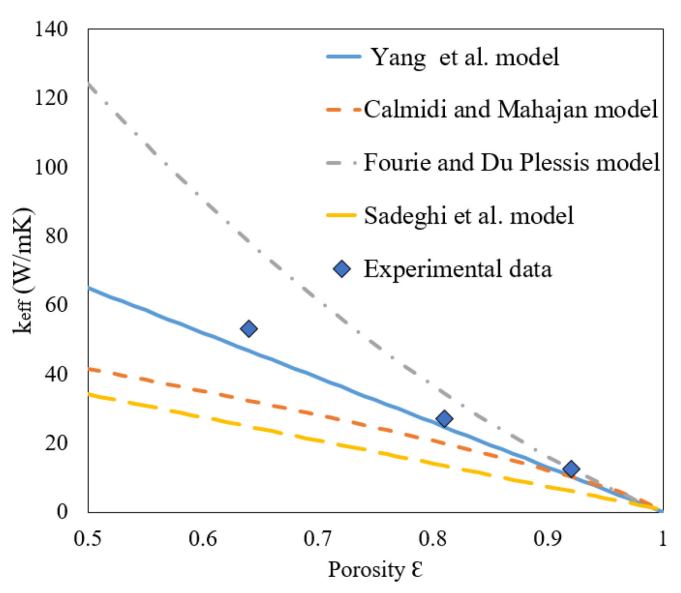


Fig. 8: Comparison of existing models with Experimental data for compressed and uncompressed Cu foam effective thermal conductivity vs. porosity at 30 Psi apparent pressure

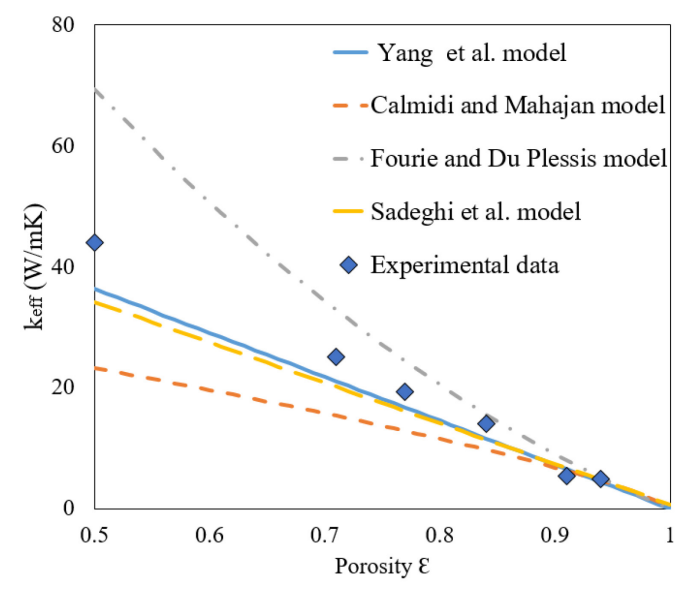


Fig. 9: Comparison of existing models with Experimental data for Al foam effective thermal conductivity vs. porosity at 30

Psi apparent pressure

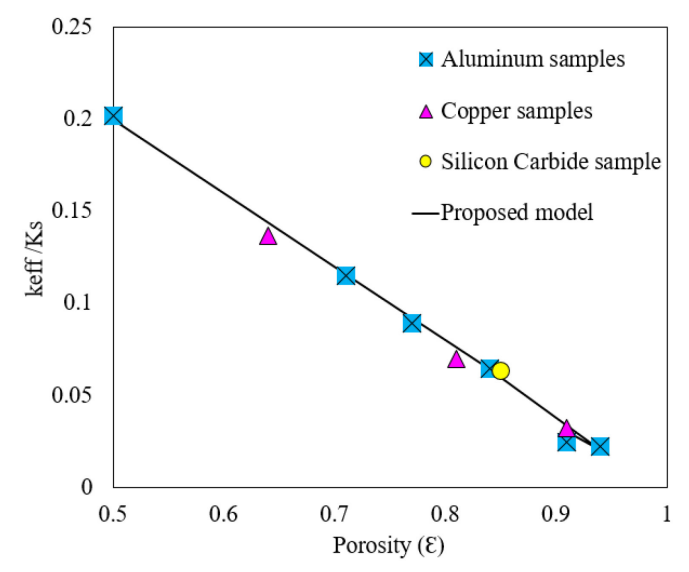


Fig. 10: Comparison of proposed models with experimental data for compressed Cu, Al and SiC foam

All of the measured effective thermal conductivities are plotted in Fig. 10 versus porosity, and compared to the model of Eq. 9. The agreement is excellent, with an RMS error of 1% over all the data. We note that the Yang's model is identical to Eq. 9, except that the 2/5 factor is replaced by 1/3.

#### D. Contact Resistance

The contact resistance variation for copper foam samples with CR of 1, 2, and 4 with TIM and without TIM is shown in Fig. 11 and Fig. 12 respectively when 30 Psi apparent pressure. It is evident that contact resistance is significantly impacted by the compression ratio. As compression rises, the actual contact area at the foam-solid interface also increases, leading to a significant decrease in contact resistance. Assuming that the foam surface area across any plane scales with the porosity, then, the contact area can be shown to be:

$$A_{contact} = (1 - \varepsilon) A_{apparent} \tag{10}$$

The apparent contact pressure is thus:

$$P_{contact} = \frac{F_{apparent}}{A_{contact}} \tag{11}$$

As predicted, Figs. 11 and 12 show that contact resistance decreases with increasing compression and decreasing porosity, both with and without a TIM material at the interface.

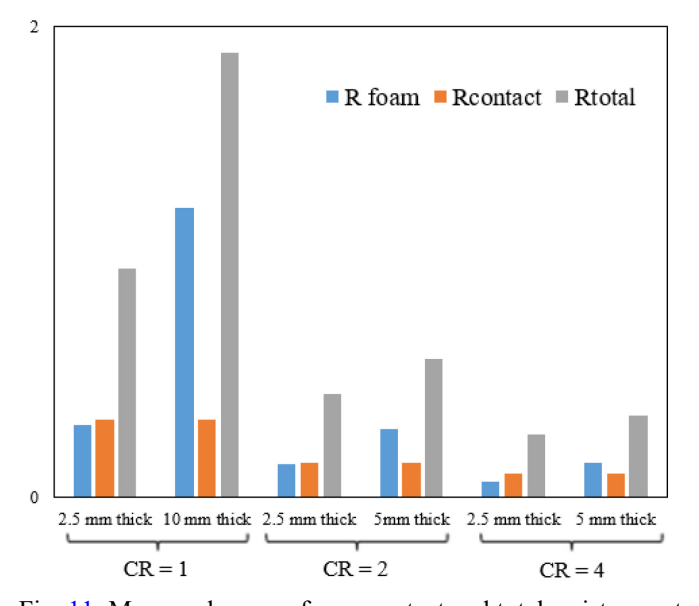


Fig. 11: Measured copper foam, contact and total resistance at 30 Psi apparent contact pressure with TIM

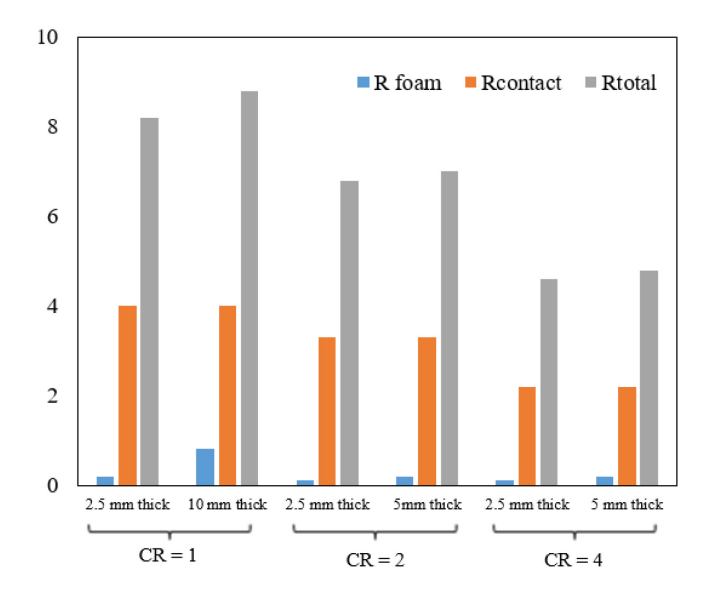


Fig. 12: Measured copper foam, contact and total resistance at 30 Psi apparent contact pressure without TIM

Fig. 13 compares the contact resistance measured for the copper foam from the present study taken at 30 psi (0.21 MPa) loading pressure to the experimental data of Sadeghi et al. [25] for uncompressed aluminum foam, acquired at approximately 47 Psi (0.33 MPa). The contact resistance has two components: the interfacial resistance between the adjacent contacting surfaces, and the constriction resistance due to the constriction of the heat flow lines into the discrete foam surface areas in contact with the continuous base to which it is mounted. The data of Fig. 13 is remarkably consistent between the recent data on Cu foam, compared to the published data on aluminum foam, indicating that the constriction resistance scales with porosity for both sets of data and that the interfacial resistance is similar.

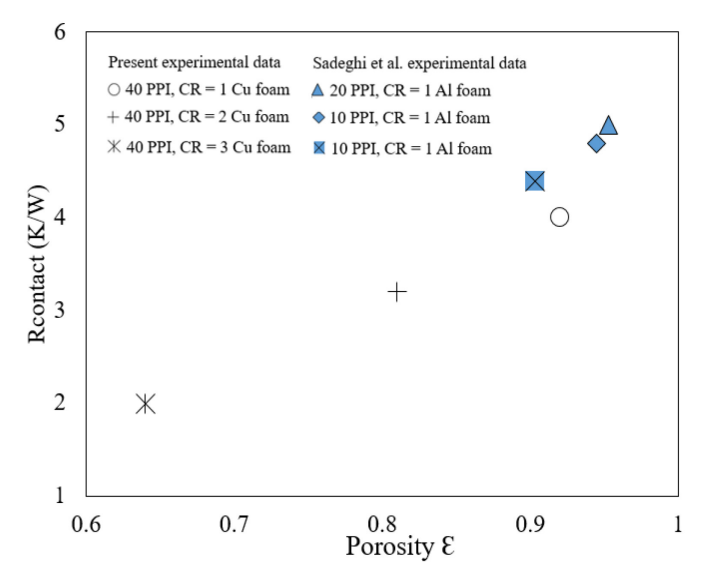


Fig. 13: Comparison of present experimental data of contact resistance with existing experimental data for samples without TIM [25]

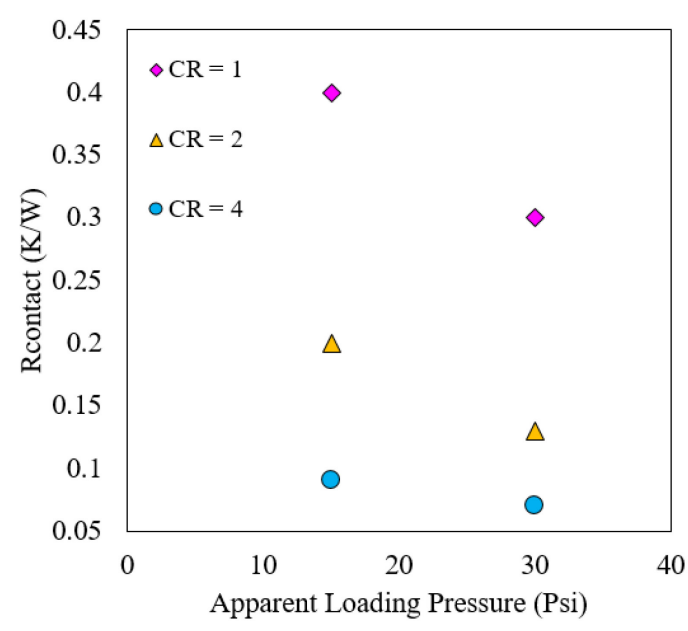


Fig. 14: Measured contact resistance for copper foam at 15 Psi and 30 Psi apparent contact pressure with TIM

Figures 14 and 15 illustrate the impact of loading pressure on contact resistance at 15 Psi and 30 Psi, both with and without a TIM. The contact resistance is notably greater at 15 Psi compared to 30 Psi. As the apparent contact pressure increases, there is a noticeable decrease in contact resistance. This trend aligns with the observations made by Sadeghi et al. [25], who asserted that the actual contact area at the interface between foam and solid expands with an increase in compressive load, resulting in a substantial reduction in contact resistance, also seen in Eq. 10

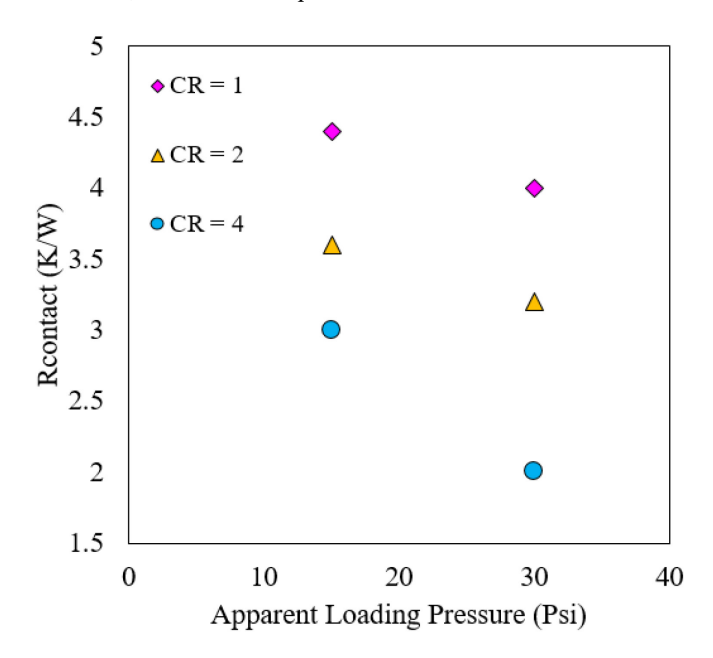


Fig. 15: Measured contact resistance for copper foam at 15 Psi and 30 Psi apparent contact pressure without TIM

# V. CONCLUSIONS

- 1. The measured thermal conductivity of uncompressed foam aligned with the expected values from a widely accepted correlation.
- The measured thermal conductivity of compressed foam exhibited an increase as porosity decreased, deviating from the accepted correlation established for uncompressed foam.
- 3. A new simple analytical model between thermal conductivity and porosity was introduced for predicting the effective thermal conductivity of compressed metal foams.
- 4. Contact resistance without TIM exceeded that with TIM, and there was a discernible reduction in contact resistance with increased loading pressure. The contact resistance exhibits an increase corresponding to an increase in porosity of the metal foam.
- 5. The measured thermal conductivity demonstrated independence from the Thermal Interface Material (TIM) utilized.

#### **ACKNOWLEDGEMENTS**

This research is supported by the National Science Foundation Industry/University Collaborative Research Center (NSF I/UCRC) under Grant No. IIP-1738782. The opinions, findings, and conclusions expressed in this article are the sole responsibility of the authors and do not necessarily reflect the official views of the NSF. Recognition is also given to ERG Aerospace Corporation for providing the uncompressed and compressed copper, aluminum and silicon carbide foam test samples and contributing to the construction of the test section. Finally, the research contributions of Ryan Plickys and Ana Ramirez to this work are highly acknowledged.

### REFERENCES

- [1] D. Kisitu, A. Ortega, M. Zlatinov, and D. Schaffarzick, "Two-phase flow in compressed copper foam with R134a for high heat flux thermal management: Effects of foam compression ratio and refrigerant operating conditions on thermohydraulic performance," in 2023 22nd IEEE Intersociety Conference on Thermal and Thermomechanical Phenomena in Electronic Systems (ITherm), May 2023, pp. 1–10. doi: 10.1109/ITherm55368.2023.10177584.
- [2] D. Kisitu and A. Ortega, "Thermal-Hydraulic Analytical Models of Split-Flow Microchannel Liquid-Cooled Cold Plates with Flow Impingement," in ASME 2021 International Technical Conference and Exhibition on Packaging and Integration of Electronic and Photonic Microsystems, Virtual, Online: American Society of Mechanical Engineers, Oct. 2021, p. V001T02A015. doi: 10.1115/IPACK2021-73283.
- [3] W. H. Hsieh, J. Y. Wu, W. H. Shih, and W. C. Chiu, "Experimental investigation of heat-transfer characteristics of aluminum-foam heat sinks," *International Journal of Heat and*

- *Mass Transfer*, vol. 47, no. 23, pp. 5149–5157, Nov. 2004, doi: 10.1016/j.ijheatmasstransfer.2004.04.037.
- [4] "Full article: Thermal Applications of Open-Cell Metal Foams." Accessed: Jun. 15, 2023. [Online]. Available: https://www.tandfonline.com/doi/full/10.1081/AMP-200030568
- [5] P. Wang, D. Y. Liu, and C. Xu, "Numerical study of heat transfer enhancement in the receiver tube of direct steam generation with parabolic trough by inserting metal foams," *Applied Energy*, vol. 102, pp. 449–460, Feb. 2013, doi: 10.1016/j.apenergy.2012.07.026.
- [6] W. Yuan, Y. Tang, X. Yang, and Z. Wan, "Porous metal materials for polymer electrolyte membrane fuel cells A review," *Applied Energy*, vol. 94, pp. 309–329, Jun. 2012, doi: 10.1016/j.apenergy.2012.01.073.
- [7] A. Lomte, B. Sharma, M. Drouin, and D. Schaffarzick, "Sound absorption and transmission loss properties of opencelled aluminum foams with stepwise relative density gradients," *Applied Acoustics*, vol. 193, p. 108780, May 2022, doi: 10.1016/j.apacoust.2022.108780.
- [8] X. Yu, Z. Lu, and W. Zhai, "Enhancing the flow resistance and sound absorption of open-cell metallic foams by creating partially-open windows," *Acta Materialia*, vol. 206, p. 116666, Mar. 2021, doi: 10.1016/j.actamat.2021.116666.
- [9] T. Piazera de Carvalho, "Two-phase flow in open-cell metal foams with application to aero-engine separators." Accessed: Dec. 26, 2023. [Online]. Available: https://eprints.nottingham.ac.uk/37062/
- [10] T. P. de Carvalho, H. P. Morvan, and D. Hargreaves, "Pore-Level Numerical Simulation of Open-Cell Metal Foams With Application to Aero Engine Separators," presented at the ASME Turbo Expo 2014: Turbine Technical Conference and Exposition, American Society of Mechanical Engineers Digital Collection, Sep. 2014. doi: 10.1115/GT2014-26402.
- [11] S. T. Kolaczkowski, S. Awdry, T. Smith, D. Thomas, L. Torkuhl, and R. Kolvenbach, "Potential for metal foams to act as structured catalyst supports in fixed-bed reactors," *Catalysis Today*, vol. 273, pp. 221–233, Sep. 2016, doi: 10.1016/j.cattod.2016.03.047.
- [12] S. Mellouli, H. Dhaou, F. Askri, A. Jemni, and S. Ben Nasrallah, "Hydrogen storage in metal hydride tanks equipped with metal foam heat exchanger," *International Journal of Hydrogen Energy*, vol. 34, no. 23, pp. 9393–9401, Dec. 2009, doi: 10.1016/j.ijhydene.2009.043.
- [13] B. Ozmat, B. Leyda, and B. Benson, "Thermal Applications of Open-Cell Metal Foams," *Materials and Manufacturing Processes*, vol. 19, no. 5, pp. 839–862, Oct. 2004, doi: 10.1081/AMP-200030568.
- [14] P. Samudre and S. V. Kailas, "Thermal performance enhancement in open-pore metal foam and foam-fin heat sinks for electronics cooling," *Applied Thermal Engineering*, vol. 205, p. 117885, Mar. 2022, doi: 10.1016/j.applthermaleng.2021.117885.
- [15] T. J. Lu, H. A. Stone, and M. F. Ashby, "Heat transfer in open-cell metal foams," *Acta Materialia*, vol. 46, no. 10, pp. 3619–3635, Jun. 1998, doi: 10.1016/S1359-6454(98)00031-7.

- [16] E. Bianchi, T. Heidig, C. G. Visconti, G. Groppi, H. Freund, and E. Tronconi, "An appraisal of the heat transfer properties of metallic open-cell foams for strongly exo-/endothermic catalytic processes in tubular reactors," *Chemical Engineering Journal*, vol. 198–199, pp. 512–528, Aug. 2012, doi: 10.1016/j.cej.2012.05.045.
- [17] M. S. Phanikumar and R. L. Mahajan, "Non-Darcy natural convection in high porosity metal foams," *International Journal of Heat and Mass Transfer*, vol. 45, no. 18, pp. 3781–3793, Aug. 2002, doi: 10.1016/S0017-9310(02)00089-3.
- [18] K. Boomsma and D. Poulikakos, "On the effective thermal conductivity of a three-dimensionally structured fluid-saturated metal foam," *International Journal of Heat and Mass Transfer*, vol. 44, no. 4, pp. 827–836, Feb. 2001, doi: 10.1016/S0017-9310(00)00123-X.
- [19] H. Yang, Y. Li, Y. Yang, D. Chen, and Y. Zhu, "Effective thermal conductivity of high porosity open-cell metal foams," *International Journal of Heat and Mass Transfer*, vol. 147, p. 118974, Feb. 2020, doi: 10.1016/j.ijheatmasstransfer.2019.118974.
- [20] J. W. Paek, B. H. Kang, S. Y. Kim, and J. M. Hyun, "Effective Thermal Conductivity and Permeability of Aluminum Foam Materials1," *International Journal of Thermophysics*, vol. 21, no. 2, pp. 453–464, Mar. 2000, doi: 10.1023/A:1006643815323.
- [21] V. V. Calmidi and R. L. Mahajan, "Forced Convection in High Porosity Metal Foams," *Journal of Heat Transfer*, vol. 122, no. 3, pp. 557–565, Feb. 2000, doi: 10.1115/1.1287793.
- [22] A. Bhattacharya, V. V. Calmidi, and R. L. Mahajan, "Thermophysical properties of high porosity metal foams," *International Journal of Heat and Mass Transfer*, vol. 45, no. 5, pp. 1017–1031, Feb. 2002, doi: 10.1016/S0017-9310(01)00220-4.
- [23] Z. Dai, K. Nawaz, Y. G. Park, J. Bock, and A. M. Jacobi, "Correcting and extending the Boomsma–Poulikakos effective thermal conductivity model for three-dimensional, fluid-saturated metal foams," *International Communications in Heat and Mass Transfer*, vol. 37, no. 6, pp. 575–580, Jul. 2010, doi: 10.1016/j.icheatmasstransfer.2010.01.015.
- [24] P. Ranut, "On the effective thermal conductivity of aluminum metal foams: Review and improvement of the available empirical and analytical models," *Applied Thermal Engineering*, vol. 101, pp. 496–524, May 2016, doi: 10.1016/j.applthermaleng.2015.09.094.
- [25] E. Sadeghi, S. Hsieh, and M. Bahrami, "Thermal conductivity and contact resistance of metal foams," *J. Phys. D: Appl. Phys.*, vol. 44, no. 12, p. 125406, Mar. 2011, doi: 10.1088/0022-3727/44/12/125406.
- [26] V. V. Calmidi and R. L. Mahajan, "The Effective Thermal Conductivity of High Porosity Fibrous Metal Foams," *Journal of Heat Transfer*, vol. 121, no. 2, pp. 466–471, May 1999, doi: 10.1115/1.2826001.
- [27] R. Singh and H. S. Kasana, "Computational aspects of effective thermal conductivity of highly porous metal foams," *Applied Thermal Engineering*, vol. 24, no. 13, pp. 1841–1849, Sep. 2004, doi: 10.1016/j.applthermaleng.2003.12.011.

- [28] "Effective thermal conductivity of porous media." Accessed: Dec. 26, 2023. [Online]. Available: https://ouci.dntb.gov.ua/en/works/45vPz8kl/
- [29] R. Dyga and W. Stanislaw, "Investigation of Effective Thermal Conductivity Aluminum Foams," *Procedia Engineering*, vol. 42, pp. 1088–1099, Dec. 2012, doi: 10.1016/j.proeng.2012.07.500.
- [30] X. Xiao, P. Zhang, and M. Li, "Preparation and thermal characterization of paraffin/metal foam composite phase change material," *Applied Energy*, vol. 112, no. C, pp. 1357–1366, 2013.
- [31] X. Xiao, P. Zhang, and M. Li, "Effective thermal conductivity of open-cell metal foams impregnated with pure paraffin for latent heat storage," *International journal of thermal sciences*, vol. 81, no. 81, pp. 94–105, 2014, doi: 10.1016/j.ijthermalsci.2014.03.006.
- [32] D. Kisitu, C. Caceres, M. Zlatinov, D. Schaffarzick, and A. Ortega, "Experimental Investigation of R134a Flow Boiling in Copper Foam Evaporators for High Heat Flux Electronics Cooling," presented at the ASME 2022 International Technical Conference and Exhibition on Packaging and Integration of Electronic and Photonic Microsystems, American Society of Mechanical Engineers Digital Collection, Dec. 2022. doi: 10.1115/IPACK2022-97400.

- [33] S. Mahjoob and K. Vafai, "A synthesis of fluid and thermal transport models for metal foam heat exchangers," *International Journal of Heat and Mass Transfer*, vol. 51, no. 15, pp. 3701–3711, Jul. 2008, doi: 10.1016/j.ijheatmasstransfer.2007.12.012.
- [34] "An Introduction to Error Analysis: The Study of Uncertainties in Physical Measurements, Third Edition," University Science Books. Accessed: Dec. 26, 2023. [Online]. Available: https://uscibooks.aip.org/books/an-introduction-to-error-analysis-the-study-of-uncertainties-in-physical-measurements-third-edition/
- [35] X. H. Yang, J. J. Kuang, T. J. Lu, F. S. Han, and T. Kim, "A simplistic analytical unit cell based model for the effective thermal conductivity of high porosity open-cell metal foams," *J. Phys. D: Appl. Phys.*, vol. 46, no. 25, p. 255302, Jun. 2013, doi: 10.1088/0022-3727/46/25/255302.
- [36] J. G. Fourie and J. P. Du Plessis, "Effective and coupled thermal conductivities of isotropic open-cellular foams," *AIChE Journal*, vol. 50, no. 3, pp. 547–556, Mar. 2004, doi: 10.1002/aic.10049.